Hindawi Publishing Corporation
International Journal of Antennas and Propagation
Volume 2015, Article ID 918698, 10 pages
http://dx.doi.org/10.1155/2015/918698

Research Article

Biotelemetric Wireless Intracranial Pressure Monitoring: An *In Vitro* Study

Mohammad H. Behfar, Toni Björninen, Elham Moradi, Lauri Sydänheimo, and Leena Ukkonen

Department of Electronics and Communications Engineering, Tampere University of Technology, 33720 Tampere, Finland

Correspondence should be addressed to Mohammad H. Behfar; mohammadhossein.behfar@tut.fi

Received 7 September 2015; Accepted 5 November 2015

Academic Editor: Apostolos Georgiadis

Assessment of intracranial pressure (ICP) is of great importance in management of traumatic brain injuries (TBIs). The existing clinically established ICP measurement methods require catheter insertion in the cranial cavity. This increases the risk of infection and hemorrhage. Thus, noninvasive but accurate techniques are attractive. In this paper, we present two wireless, batteryless, and minimally invasive implantable sensors for continuous ICP monitoring. The implants comprise ultrathin (50 μm) flexible spiral coils connected in parallel to a capacitive microelectromechanical systems (MEMS) pressure sensor. The implantable sensors are inductively coupled to an external on-body reader antenna. The ICP variation can be detected wirelessly through measuring the reader antenna's input impedance. This paper also proposes novel implant placement to improve the efficiency of the inductive link. In this study, the performance of the proposed telemetry system was evaluated in a hydrostatic pressure measurement setup. The impact of the human tissues on the inductive link was simulated using a 5 mm layer of pig skin. The results from the *in vitro* measurement proved the capability of our developed sensors to detect ICP variations ranging from 0 to 70 mmHg at 2.5 mmHg intervals.

1. Introduction

Management of elevated intracranial pressure (ICP) is an essential care in patients suffering from traumatic brain injuries (TBI) [1]. Increased ICP is characterized as neurological disorder which is commonly caused as a consequence of cerebral edema, cerebrospinal fluid disorders, head injury, and localized intracranial mass lesion [2]. The normal ICP value for adults lies within 10 to 15 mmHg [1]. Intractable intracranial hypertension (IH) may increase the risk of severe brain damage, disability, or death. In clinical routine, there are direct invasive and indirect noninvasive methods for management of raised ICP. Interventricular catheters are commonly used in clinical ICP measurement. Nevertheless, catheter insertion introduces the risk of hemorrhage and infection [3, 4]. On the other hand, indirect noninvasive methods such as magnetic resonance imaging (MRI), analysis of electroencephalograph (EEG) power spectrum, and audiological and ophthalmological techniques are less accurate compared to the invasive methods [5]. Recently, a newly developed noninvasive ICP monitoring device was introduced by Headsens Ltd. The device utilizes acoustic waves to assess ICP. A low frequency acoustic signal is transmitted in one ear and received in other ear. The received data is processed and analyzed to calculate the intracranial pressure [6]. Clinical performance of the device is under investigation [7].

In order to surmount the complications of the existing invasive ICP measurement methods, battery powered implantable sensors were proposed. In [8], Kawoos et al. proposed a battery supplied implantable wireless sensor. The sensor detects ICP variations through change in capacitance of a MEMS pressure sensor and the measurement data is transmitted to an external unit via 2.4 GHz RF link. In another work [9], Meng et al. reported a battery assisted implant which detects the ICP variation through

the change in oscillation frequency of an RC oscillator, which modulates a 2.4 GHz RF oscillator coupled to a planar inverted-F antenna.

The major drawback of the battery powered sensors is the increased size of the implant due to the battery and therefore the more invasive implantation. Moreover, life time of those implants is confined by the life time of the battery. Rechargeable batteries also have limited recharge cycles. Therefore, miniaturized batteryless implants are of interest for minimally invasive ICP monitoring. In a recent study [10], Chen et al. reported a mm size passive implantable sensor for continuous subdural ICP monitoring. The whole sensor is implanted under the skull and pressure variation is detected through an external reader antenna. The sensor was evaluated through an *in vivo* experiment in a rat's head. However, in the proposed inductive link, the minimum distance between the implant and reader antenna is limited to the thickness of the skin and skull. Thickness of rat skull is 0.71 ± 0.03 mm whereas the average thickness of human skull is found to be 6.32 mm [11, 12]. Thus, the feasibility of ICP monitoring based on coupled antennas in humans requires further investigations.

In [13], Moradi et al. analyzed a telemetry system for wireless subdural ICP monitoring. In the proposed telemetry model, a subdural capacitive MEMS pressure sensor is connected to an on-skull coil through a biocompatible transcranial feedthrough. The MEMS sensor and the coil form an LC tank whose resonance frequency changes as a function of ICP variations. Any change in the resonance frequency of the sensor and thus the ICP variation can be wirelessly detected via an on-body reader antenna which is inductively coupled to the on-skull coil.

Following the telemetry model proposed in [13], in this paper, we introduce fully implantable passive sensors for continuous ICP monitoring. Our research aims to simulate realistic conditions for ICP measurement and evaluate the effects of the dissipative dielectric properties of the human tissues on the telemetry operation. To this end, an *in vitro* experiment was performed in a liquid phase measurement setup and a 5 mm layer of pig skin was used to simulate the dielectric properties of the human skin. We also propose a novel implant placement to reduce the coupling distance between the implant and reader which results in improved link efficiency. As shown in Figure 1, the flexible spiral coil lies between the skull and skin and is connected to the MEMS sensor through an ultrathin RF coaxial cable. The deformable diaphragm of the MEMS sensor is in contact with CSF for subdural ICP measurement. Both the MEMS sensor and coaxial cable are placed in a protective chamber which improves the mechanical attachment of the implant to the skull and facilitates the implant removal in case of rejection. The protective chamber was not developed in this phase of the study. It is planned to be a biocompatible, nonmetallic cylindrical chamber to protect the MEMS sensor and cable in physiological environment after implantation. However, since the coaxial cable itself is shielded, presence of the chamber does not affect the telemetry operation.

The remainder of this paper is organized in four sections. Section 2 describes and analyzes the telemetry model for the wireless ICP monitoring. The conducted experiment and corresponding results are discussed in Sections 3 and 4, respectively. The paper concludes with the outcome as well as the future extension of the research in Section 5.

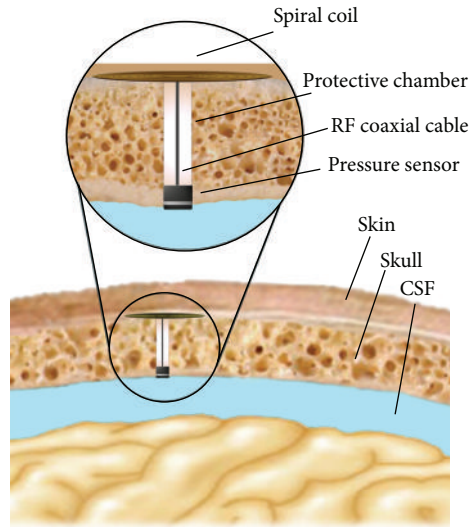

Figure 1: Conceptual illustration of the implant placement.

2. Telemetry System Description

2.1. Sensor and Wireless Operation. The wireless pressure sensing is based on near field inductive coupling between the implantable sensor and the external reader antenna. In this study, two sensors were developed with different operation frequency at 13 MHz (sensor A) and 31.2 MHz (sensor B) to investigate the effect of operation frequency on measurement sensitivity. In addition, operating at higher frequency takes advantage of smaller coil required for telemetry operation. Each sensor consists of a planar spiral coil connected in parallel to a capacitive MEMS pressure sensor (Murata SCB10H-B012FB). The spiral coils were fabricated on an ultrathin (50 μm) flexible polyimide substrate ($\varepsilon_r = 3.3$, $\tan\delta = 0.002$) to be as minimally invasive as possible for implantation. The inductance of the spiral coil (L_s) and capacitance of the MEMS sensor (C_s) form an LC tank whose resonance frequency (f_s) is determined by

$$f_s = \frac{1}{2\pi\sqrt{L_s C_s}}. \quad (1)$$

The reader antenna is a single turn loop in series with a capacitor whose resonance frequency is adjusted to the resonance frequency of the sensors. To achieve the maximum sensitivity, the reader and sensor were tuned to resonate near the same frequency. Table 1 lists the characteristics of the sensors and reader antenna. The telemetry model for the wireless ICP monitoring is shown in Figure 2(c). The reader loop is excited with an alternating current and thereby an electromagnetic (EM) field is created around the loop. When the reader loop and implantable sensor are near each other, the EM field induces a current in the sensor side loop. The current flow in the sensor side loop causes a secondary EM

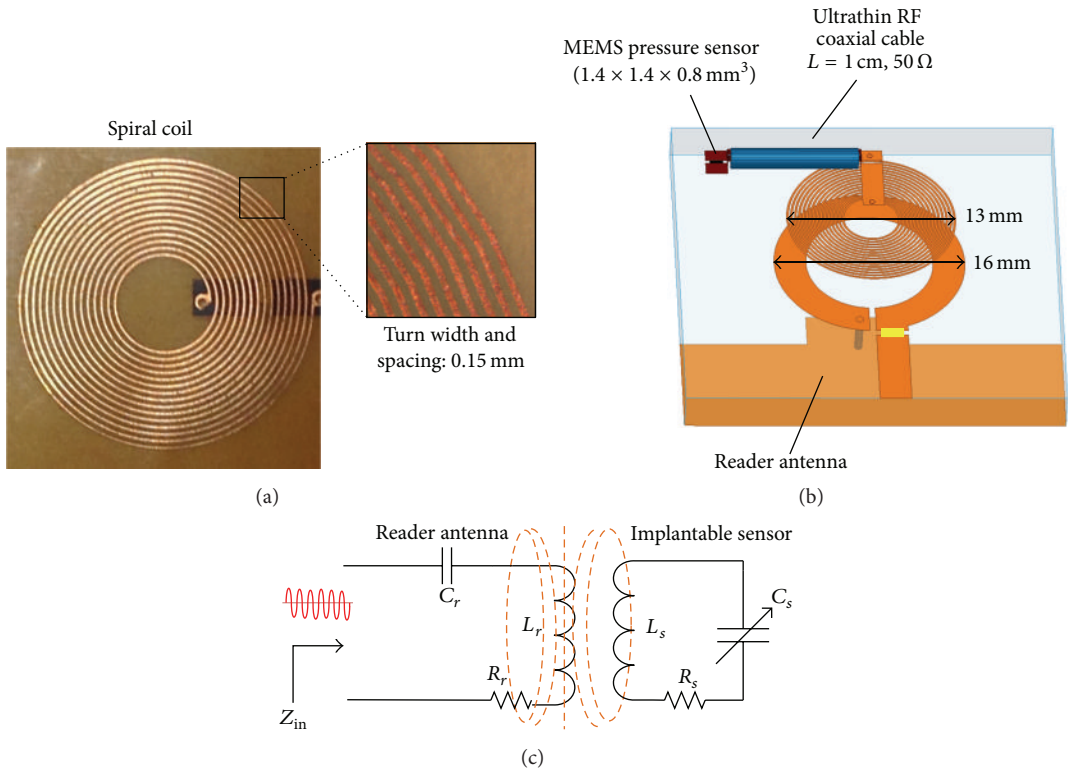

Figure 2: (a) Spiral coil of sensor B. (b) Simulated implant and reader antenna. (c) Telemetry model for wireless ICP monitoring.

Table 1: Characteristics of the sensors and reader loop.

Sensor	Resonance frequency at 0 mmHg [MHz]	Number of turns	Diameter/trace width [mm]
Sensor A	13	15	13/0.15
Sensor B	31.2	30	22/0.15
Reader antenna	14.5 (C_s = 6.8 nF) 34.2 ($C_s \approx$ 1 nF)	1	16/3

field in the surrounding of the sensor's coil which impacts the current flow in the reader loop. In Figure 2(c), R_r and R_s represent the resistance of the reader antenna and the sensor's coil, respectively. M is the mutual inductance between L_r and L_s. To simplify the model, the series inductance and resistance of the coaxial cable are included in L_s and R_s, respectively. Through the circuit analysis described in [17], the input impedance (Z_{in}) of the reader antenna can be expressed by

$$Z_{in} = R_r + j\omega L_r + \frac{1}{j\omega C_r} - \frac{(j\omega M)^2}{j\omega L_s + 1/j\omega C_s + R_s}. \quad (2)$$

By substituting $M = K\sqrt{L_r L_s}$ and considering the resonance condition where $L_r C_r = 1/4\pi^2 f_r^2$ and $L_s C_s = 1/4\pi^2 f_s^2$, the total input impedance seen from the reader antenna's input is given by [17]

$$Z_{in} = R_r + j\omega L_r \left[1 - \left(\frac{f_r}{f}\right) + \frac{K^2 (f/f_s)^2}{1 - (f/f_s)^2 + \left(jR_s/\sqrt{L_s/C_s}\right)(f/f_s)}\right], \quad (3)$$

where f is the frequency of the excitation signal and f_r is the resonance frequency of the reader. K denotes the coupling coefficient of the inductive link. According to (2) and (3), Z_{in} changes as a function of pressure variation and its sensitivity toward C_s highly depends on K which is determined by several factors such as the dielectric material and distance between the coils, the mutual alignments, and geometry and ohmic losses of the coils [13].

When the implantable sensor is excited at its resonance frequency ($f = f_s$), the input impedance can be written as

$$Z_{\text{in}} = R_r + \omega L_r \frac{K^2}{R_s}\sqrt{\frac{L_s}{C_s}} + j\omega L_r\left[1 - \left(\frac{f_r}{f}\right)\right]. \quad (4)$$

Accordingly, the impedance phase at resonance condition is given by

$$\begin{aligned}\angle Z_{\text{in}} &= \tan^{-1}\left[\frac{X_{\text{in}}}{R_{\text{in}}}\right] \\ &= \tan^{-1}\left[\frac{\omega L_r\left[1-\left(f_r/f\right)\right]}{R_r + \omega L_r\left(K^2/R_s\right)\sqrt{L_s/C_s}}\right],\end{aligned} \quad (5)$$

where R_{in} and X_{in} are the resistive and reactive parts of the input impedance, respectively. Equation (5) states that any change in the capacitance of the MEMS sensor and thus in the resonance frequency of the implantable sensor impacts the impedance phase.

Considering the inductively coupled sensor and reader antenna as a complex load at the end of a transmission line with characteristics impedance of Z_o, the reflection coefficient is defined as

$$\Gamma = \frac{Z_{\text{in}} - Z_o}{Z_{\text{in}} + Z_o} = \frac{R_{\text{in}} + jX_{\text{in}} - Z_o}{R_{\text{in}} + jX_{\text{in}} + Z_o}. \quad (6)$$

Splitting Γ into its real and imaginary parts yields

$$\begin{aligned}\Gamma = &\frac{R_{\text{in}}^2 - Z_o^2 + X_{\text{in}}^2}{R_{\text{in}}^2 + X_{\text{in}}^2 + Z_o^2 + 2Z_oR_{\text{in}}} \\ &+ j\frac{2Z_oX_{\text{in}}}{R_{\text{in}}^2 + X_{\text{in}}^2 + Z_o^2 + 2Z_oX_{\text{in}}}.\end{aligned} \quad (7)$$

By substituting R_{in} and X_{in} from (4) in (7), the reflection phase is expressed by

$$\varphi = \tan^{-1}\left[\frac{\text{Im}\{\Gamma\}}{\text{Re}\{\Gamma\}}\right] = \tan^{-1}\left[\frac{2Z_oX_{\text{in}}}{R_{\text{in}}^2 + X_{\text{in}}^2 - Z_o^2}\right] = \tan^{-1}\left[\frac{2Z_o\omega L_r\left[1-\left(f_r/f\right)\right]}{\left(R_r + \omega L_r\left(K^2/R_s\right)\sqrt{L_s/C_s}\right)^2 + \left[\omega L_r\left[1-\left(f_r/f\right)\right]\right]^2 - Z_o^2}\right]. \quad (8)$$

In this study, we track the changes in the resonance frequency of the sensors and impedance and reflection phase of the load as the responsive parameters to the pressure variations.

2.2. Sensitivity of the Implantable Sensors. Sensitivity of the sensors toward the pressure variation can be defined as the rate of change in the resonance frequency of the sensor with respect to the change in the capacitance of the MEMS sensor. Since the MEMS sensor's capacitance changes as a function of the imposed pressure, the sensitivity of the sensor toward the pressure variation can be expressed by [13]

$$\frac{\partial f_s}{\partial C_s} = -\frac{1}{4\pi C_s\sqrt{L_sC_s}} = -\frac{f_s}{2C_s}. \quad (9)$$

In view of (9), sensitivity increases if the implantable sensor is excited at a higher frequency. In addition, miniaturization of the implant is achievable at higher excitation frequency by reducing the number of the spiral coil's turns. However, we found by experiment that the MEMS sensor introduces noticeable parasitics above 50 MHz and, consequently, the quality factor of the resonator formed by the spiral coil and MEMS sensor reduces. Thus, the operational frequency should be reduced to a lower frequency. In this work, the implantable sensors were tuned to resonate at around 13 MHz and 31.2 MHz at normal air pressure where the nominal capacitance of the MEMS sensor is approximately 10 pF. The performance comparison of the sensors is provided in Section 4.

2.3. Simulation. In order to verify the possibility of unambiguous detection of the pressure change from the coupled reader antenna's input impedance, full-wave electromagnetic simulations were conducted using ANSYS HFSS v.15. The simulation model is depicted in Figure 2(b) for sensor B. In the simulation, the coils were placed in air at the distance of 5 mm from each other and the impact of pressure variation was simulated by modeling the MEMS pressure sensor as a variable capacitor. The results from the simulation are shown in Figure 3. Here, the simulated impedance of the reader antenna and the implantable sensor are denoted by Z_{reader} and Z_{sensor}, respectively. The resonance frequency of the sensor is seen as an upward peak in the reader antenna's input impedance. When capacitance of the MEMS sensor changes as a function of pressure variation, the resonance frequency of the sensor changes and thereby the location of the peak moves along the frequency axis. Overall, the simulation results support the feasibility of the proposed wireless sensor readout modality. The accuracy of the readout through tissue layers is attested further through experiments, which are described in the next section.

3. Experiment

3.1. Hydrostatic Pressure Measurement Setup. The sensors were evaluated in a hydrostatic pressure measurement setup, which is illustrated in Figure 4(a). In order to avoid direct contact of the coils with the skin, both sides of the sensors were coated with thin adhesive tape. The side walls of the MEMS pressure sensor were conformally coated with silicon paste to avoid water penetration into the sensing element.

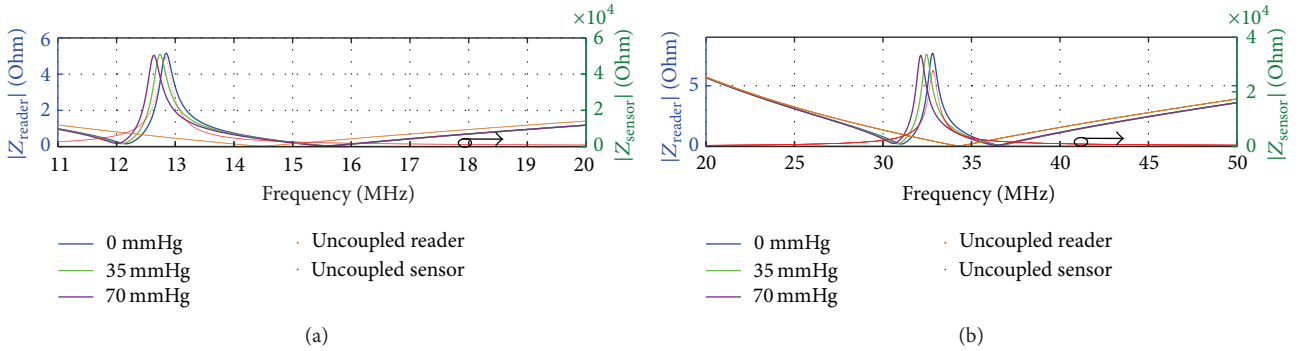

FIGURE 3: Simulated impedance of the reader antenna and implantable sensors at different pressures. The simulation results for sensor A and sensor B are shown in (a) and (b), respectively.

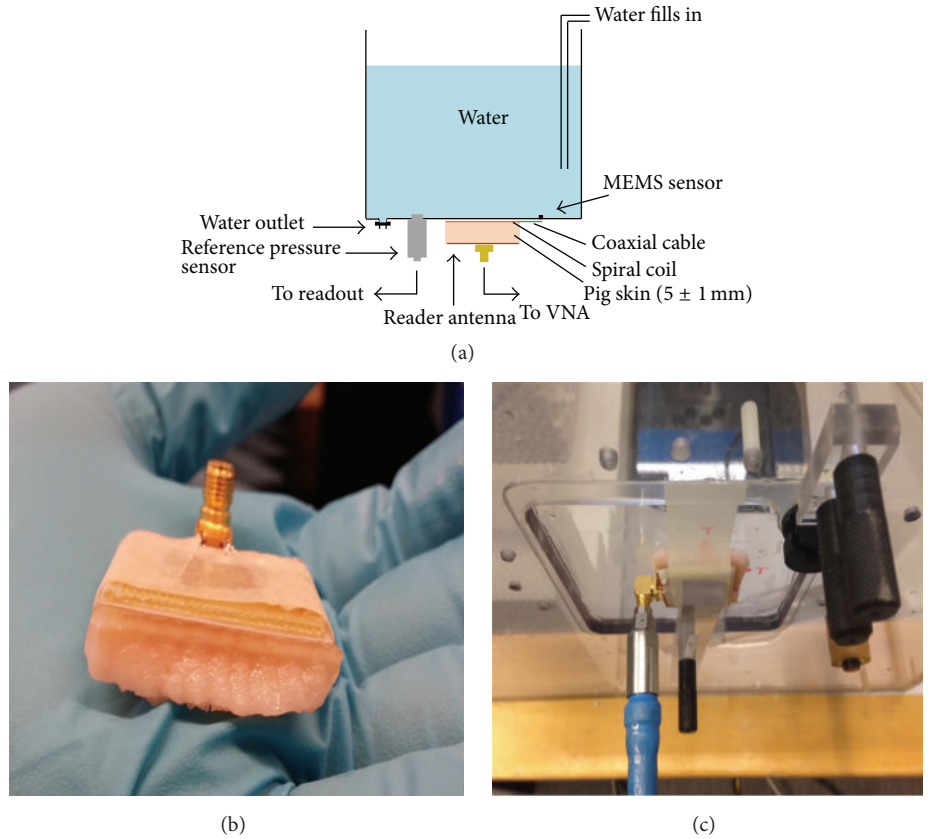

FIGURE 4: (a) Conceptual illustration of the measurement setup. (b) Pig skin attached to the reader antenna. (c) Reader antenna.

The MEMS sensor was placed inside the tank through a small opening at the bottom of the water column so that it was exposed to the hydrostatic pressure of the water column. The coils were connected to the MEMS sensor via a 1 cm RF coaxial cable, which simulates the connection of the MEMS sensor to the implanted coil in the real ICP monitoring as depicted in Figure 1. The actual pressure at the bottom of the tank was measured with electronic pressure sensor (IMF electronic gmbh PA 3528) [18]. As shown in Figure 4(c), the reader antenna was placed outside the water column and centrally aligned with the implantable sensor. The reader antenna and sensor were separated with 5 mm thick pig skin.

As mentioned previously, the pig skin is used to simulate the dielectric properties of the human skin and its impact on the efficiency of the link. According to a study on dielectric parameters of pig biological tissues [19], dielectric properties of the pig skin used in this measurement correspond best to the dielectric characteristics of the tissue in an 11–13-year-old human. As explained in Section 2, any change in the resonance characteristics of the implantable sensor can be detected through measuring the reader antenna's input impedance. To this end, 6 consecutive measurements were conducted with each sensor. The input impedance of the reader antenna was measured using a Vector Network

Analyzer (VNA) while the hydrostatic pressure of the water column was being changed within the interval from 0 to 70 mmHg with both increasing and decreasing gradients. Raised ICP is defined depending on physiological condition. In hydrocephalus, ICP greater than 15 mmHg is considered elevated. In case of head injury, ICP above 20 mmHg is regarded to be abnormal and treatment is usually started when it exceeds 25 mmHg [20]. In this study, the applied pressure is varied within 0–70 mmHg to provide adequate measurement range for ICP monitoring. All the pressure values reported in this paper are relative to the atmospheric pressure. The remainder of this paper presents the measurement results and discusses the observations.

4. Result and Discussion

The magnitude and phase angle of the reader antenna's input impedance as well as the reflection phase of the sensors are shown in Figures 5(a)–5(c) and 6(a)–6(c). As expected from the theoretical analysis and simulation results, the resonance frequency of the implant reduces as a function of increasing pressure. The impedance phase shows a dip near the resonance frequency of the sensor. The overall frequency shift of 280 kHz and 720 kHz is observed for sensor A and sensor B, respectively. The location of the minimum phase shows a linear decline when pressure increases from 0 to 70 mmHg. As seen from Figures 5(c) and 6(c), the reflection phase of the sensors changes as a function of the pressure. This is due to change in reactive characteristics of the impedance under the applied pressure. In this study, we measure the location of minimum reflection phase which corresponds to the maximum phase delay between the incident and reflected signal. In fact, this quantity represents the time domain phase delay between the incident and backscattered signal. The overall measurement results are summarized in Table 2. As it presents, the overall shift in resonance frequency of the sensors increases proportionally to the increase in the operation frequency. This is in agreement with (9). The overall change in impedance phase and reflection phase also varies as the operation frequency increases. However, higher operation frequency has no significant impact on those parameters since they are also dependent on other factors such as mutual inductance, coupling distance, and geometry of the coils. As can be seen in Figures 5(a), 5(b), 6(a) and 6(b), there is a sudden jump in the magnitude and phase of the input impedance when pressure changes from 0 to 2.5 mmHg. This can be explained by the addition of water near the sensor's coil. Water has high permittivity value and tends to reduce the electric flux around the sensor's coil, resulting in increased losses and realized impedance of the reader antenna. In the real application for ICP measurement, the spiral coil is placed between the fat layer of the head skin and skull. The permittivities of the skin and cranial bone are much less than permittivity of water. Thus, proximity of water to the coil could simulate the worst condition for evaluation of the inductive link efficiency for ICP monitoring. In fact, dielectric property of water represents the effect of dissipative properties of the skull on the telemetry operation. Table 3 compares the relevant permittivities of the tissue and water at different frequencies.

Although the simulation results are in agreement with the measurement data, it could be seen that the magnitude of the resonance peaks in the simulation is greater than the peaks in the measurement data. This can be explained by different coupling condition. In the simulation, the reader and spiral coil are placed in air at separation of 5 mm from each other whereas in the real experiment the distance between the reader and coil is filled with a 5 mm layer of pig skin. In addition, the other side of the coil is in proximity of the water of the tank. As explained earlier in this section, proximity of water to the coil attenuates the electric flux around the sensor's coil which results in reduced quality factor of the coil and, thus, lower resonance peaks seen in the results from the measurement data.

Information derived from change in the resonance frequency of the sensors could provide highly linear and repeatable pressure readout at 5 mmHg intervals in measurement with sensor A and 2.5 mmHg intervals with sensor B. Impedance phase and reflection phase could provide pressure readout at 2.5 mmHg intervals in measurement with both sensors. However, the best linearity and repeatability are obtained from the impedance phase and reflection phase of sensor B. Measurement results imply that, in a low operation frequency where the rate of change in the resonance frequency of the sensor is limited to the excitation frequency, other quantities such as impedance phase and reflection phase could be used to achieve high resolution pressure readout.

The sensor is expected to detect the trend of pressure variations. Therefore, it needs to be calibrated for each individual subject to read the sensor response at normal and elevated pressure. In this study, we mainly focused on the telemetric operation, resolution, and repeatability of the pressure readout. We acknowledge that other factors such as thermal drift, MEMS sensor's zero pressure drift, and misalignment between the reader and sensor might affect the measurement accuracy which need to be investigated in our future studies.

5. Conclusion

Performance evaluation of two fully implantable sensors for minimally invasive continuous ICP monitoring is presented. We demonstrated high resolution, linear and repeatable pressure readout at 2.5 mmHg. The sensors were evaluated in a hydrostatic pressure measurement setup to emulate the real conditions in *in vivo* ICP monitoring. The impact of the human lossy tissues on the wireless operation was simulated using a 5 mm layer of pig skin. In addition, we introduced a novel sensor structure and implant placement to reduce the coupling distance and thus improve the efficiency of the link between the on-body reader antenna and implantable sensor. Moreover, compared to the previously reported ICP sensors, our proposed sensor introduces the least invasiveness for implantation since the spiral coil lies only a few millimeters down under the head skin. The measurement results

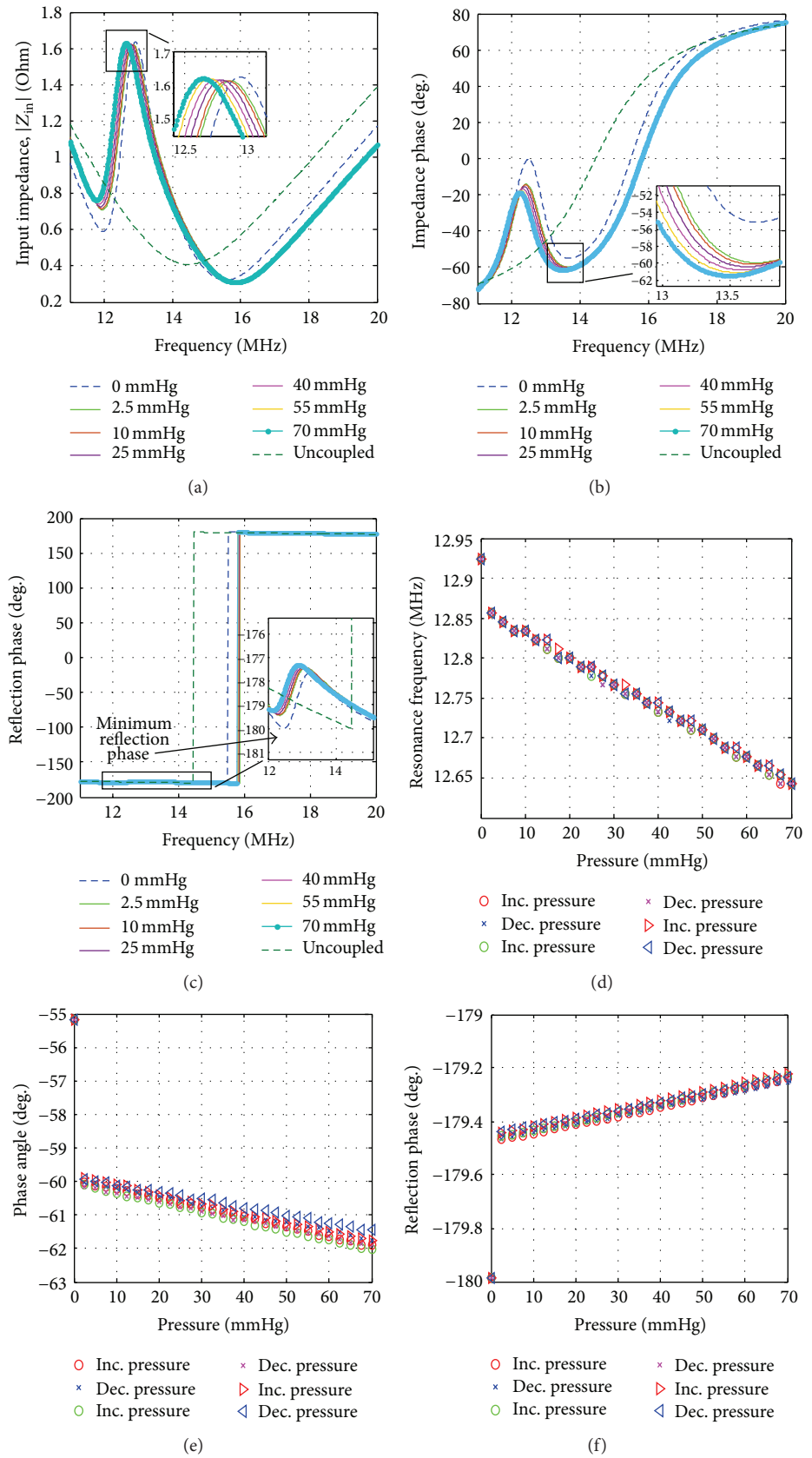

FIGURE 5: Measurement results obtained from sensor A. (a) Magnitude and (b) phase angle of the reader antenna's input impedance. (c) Reflection phase of the sensor as a variable load. (d) Shift in the resonance frequency of the sensor as a function of pressure. (e) Phase dip variation. (f) Phase shift versus applied pressure.

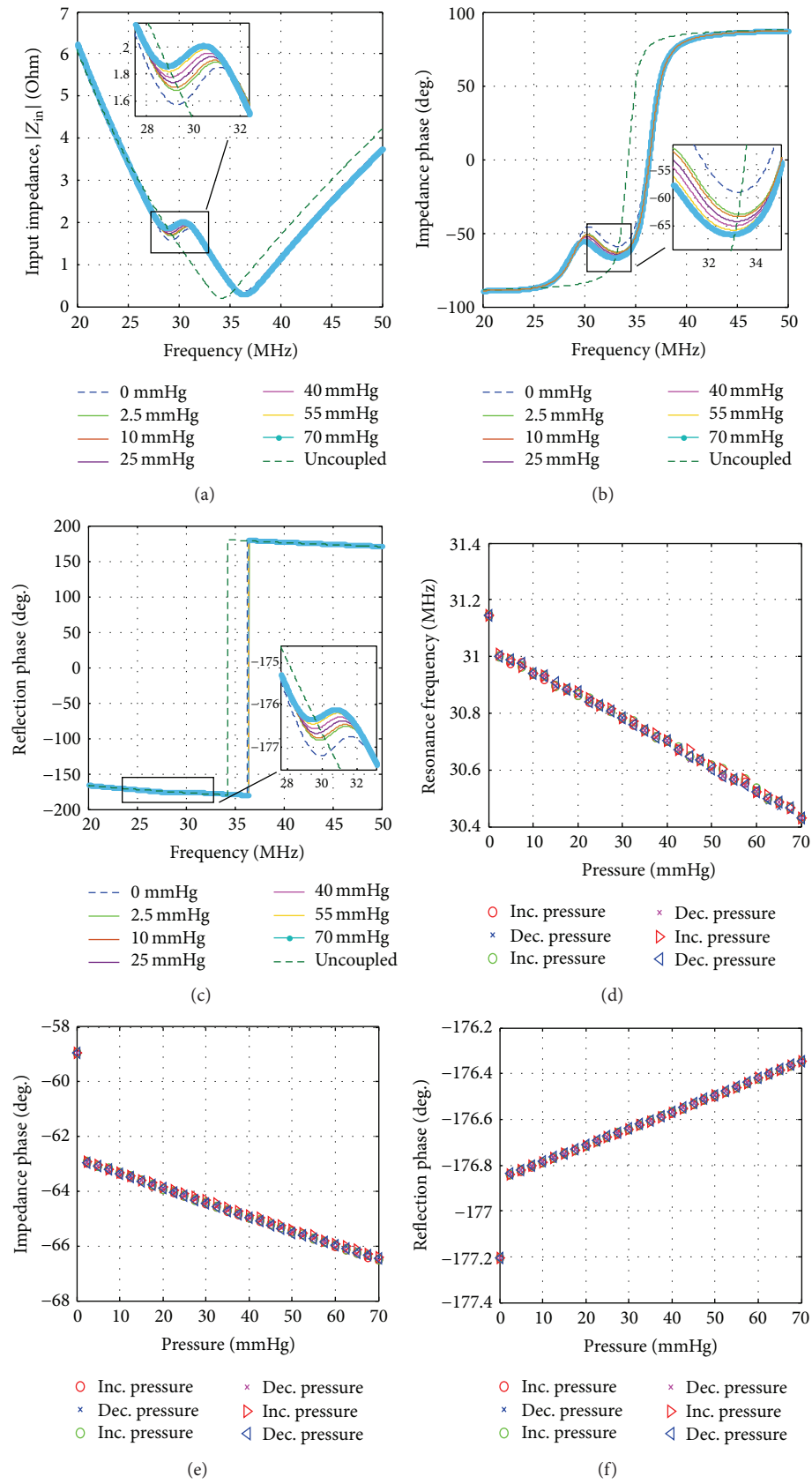

Figure 6: Measurement results obtained from sensor B. (a) Magnitude and (b) phase angle of the reader antenna's input impedance. (c) Reflection phase of the sensor as a variable load. (d) Shift in the resonance frequency of the sensor as a function of pressure. (e) Phase dip variation. (f) Phase shift versus applied pressure.

Table 2: Summary of the measurement results.

Sensor	Resonance frequency [MHz]	Overall shift in resonance frequency [kHz]	Overall phase dip change [degree]	Overall reflection phase change [degree]	Max. resolution from resonance frequency [mmHg]	Max. resolution from impedance phase [mmHg]	Max. resolution from reflection phase [mmHg]
A	13	280	6.84	0.8	5	2.5	2.5
B	31.2	720	7.51	0.9	2.5	2.5	2.5

Table 3: Dielectric properties of the tissues and water [14–16].

Tissue	Relative permittivity	Conductivity [S/m]
Skin (fat layer)	12.08 (at 13 MHz) 7.91 (at 32 MHz)	0.030 (at 13 MHz) 0.033 (at 32 MHz)
Skull (compact bone)	31.33 (at 12 MHz) 20.44 (at 32 MHz)	0.045 (at 13 MHz) 0.053 (at 32 MHz)
Water	≈80 (at 20°C)	0.005–0.05

imply that operating at higher frequency could improve the sensitivity of the measurement which results in higher resolution pressure readout. In addition, it benefits further miniaturization of the sensors. The results also suggest that the most linear pressure readout can be derived from the reflection phase of the sensor as well as the impedance phase of the reader antenna. In the current studies of LC resonant sensors for wireless sensing of the physiological parameters, the wireless readout is usually performed by a high frequency measurement instrument, such as VNA or impedance analyzer. However, clinical utilization of this kind of sensors requires dedicated readout electronics for wireless sensing of the desired parameters. Findings from this study suggest that high precision phase comparators could be a promising approach to develop a customized wireless readout system for continuous ICP monitoring.

Conflict of Interests

The authors declare that there is no conflict of interests regarding the publication of this paper.

Acknowledgments

This work was supported by the Academy of Finland (Funding Decisions 265768, 258460, and 264947), Jane and Aatos Erkko Foundation, and the Finnish Funding Agency for Technology and Innovation (TEKES). The authors thank Nazanin Zanjanizadeh Ezazi for her contribution to the graphical illustration of the brain tissue.

References

[1] R. M. Chesnut, N. Temkin, N. Carney et al., "A trial of intracranial-pressure monitoring in traumatic brain injury," *The New England Journal of Medicine*, vol. 367, no. 26, pp. 2471–2481, 2012.

[2] L. T. Dunn, "Raised intracranial pressure," *Journal of Neurology, Neurosurgery & Psychiatry*, vol. 73, supplement 1, pp. i23–i27, 2002.

[3] C. Wiegand and P. Richards, "Measurement of intracranial pressure in children: a critical review of current methods," *Developmental Medicine and Child Neurology*, vol. 49, no. 12, pp. 935–941, 2007.

[4] P. H. Raboel, J. Bartek, M. Andresen, B. M. Bellander, and B. Romner, "Intracranial pressure monitoring: invasive versus non-invasive methods—a review," *Critical Care Research and Practice*, vol. 2012, Article ID 950393, 14 pages, 2012.

[5] H. Kristiansson, E. Nissborg, J. Bartek, M. Andresen, P. Reinstrup, and B. Romner, "Measuring elevated intracranial pressure through noninvasive methods: a review of the literature," *Journal of Neurosurgical Anesthesiology*, vol. 25, no. 4, pp. 372–385, 2013.

[6] Headsense, "Headsense," http://www.head-sense-med.com/.

[7] "An evaluation of non-invasive ICP monitoring in patients undergoing invasive ICP monitoring via an external ventricular drainage (EVD) device," https://clinicaltrials.gov/ct2/show/NCT02284217.

[8] U. Kawoos, M.-R. Tofighi, R. Warty, F. A. Kralick, and A. Rosen, "In-vitro and in-vivo trans-scalp evaluation of an intracranial pressure implant at 2.4 GHz," *IEEE Transactions on Microwave Theory and Techniques*, vol. 56, no. 10, pp. 2356–2365, 2008.

[9] X. Meng, K. Browne, S. M. Huang, D. K. Cullen, M. R. Tofighi, and A. Rosen, "Dynamic study of wireless intracranial pressure monitoring of rotational head injury in swine model," *Electronics Letters*, vol. 48, no. 7, pp. 363–364, 2012.

[10] L. Y. Chen, B. C.-K. Tee, A. L. Chortos et al., "Continuous wireless pressure monitoring and mapping with ultra-small passive sensors for health monitoring and critical care," *Nature Communications*, vol. 5, article 5028, 2014.

[11] M. A. O'Reilly, A. Muller, and K. Hynynen, "Ultrasound insertion loss of rat parietal bone appears to be proportional to animal mass at submegahertz frequencies," *Ultrasound in Medicine and Biology*, vol. 37, no. 11, pp. 1930–1937, 2011.

[12] A. Moreira-Gonzalez, F. E. Papay, and J. E. Zins, "Calvarial thickness and its relation to cranial bone harvest," *Plastic and Reconstructive Surgery*, vol. 117, no. 6, pp. 1964–1971, 2006.

[13] E. Moradi, T. Björninen, L. Sydänheimo, and L. Ukkonen, "Analysis of biotelemetric interrogation of chronically implantable intracranial capacitive pressure sensor," in *Proceedings of the IEEE RFID Technology and Applications Conference (RFID-TA '14)*, pp. 145–149, Tampere, Finland, September 2014.

[14] Institute for Applied Physics, "An Internet resource for the calculation of the Dielectric Properties of Body Tissues," http://niremf.ifac.cnr.it/tissprop/htmlclie/htmlclie.php.

[15] W. J. Ellison, K. Lamkaouchi, and J.-M. Moreau, "Water: a dielectric reference," *Journal of Molecular Liquids*, vol. 68, no. 2-3, pp. 171–279, 1996.

[16] Water treatment and purification—Lenntech, http://www.lenntech.com/.

[17] Z. Huixin, H. Yingping, G. Binger, L. Ting, X. Jijun, and Z. Huixin, "A readout system for passive pressure sensors," *Journal of Semiconductors*, vol. 34, no. 12, 2013.

[18] "PA3528—Electronic pressure sensor—eclass: 27201302/27-20-13-02," http://www.ifm.com/products/gb/ds/PA3528.htm.

[19] A. Peyman, C. Gabriel, E. H. Grant, G. Vermeeren, and L. Martens, "Variation of the dielectric properties of tissues with age: the effect on the values of SAR in children when exposed to walkie-talkie devices," *Physics in Medicine and Biology*, vol. 54, no. 2, pp. 227–241, 2009.

[20] M. Czosnyka and J. D. Pickard, "Monitoring and interpretation of intracranial pressure," *Journal of Neurology, Neurosurgery and Psychiatry*, vol. 75, no. 6, pp. 813–821, 2004.